CHANNELS
2022, VOL. 16, NO. 1, 72–83
https://doi.org/10.1080/19336950.2022.2053420

Taylor & Francis
Taylor & Francis Group

RESEARCH PAPER

OPEN ACCESS Check for updates

Effects of JZTX-V on the wild type Kv4.3 Expressed in HEK293T and Molecular Determinants in the Voltage-sensing Domains of Kv4.3 Interacting with JZTX-V

Xu Dehong[a,b], Wu Wenmei[a], Hong Siqin[a], Zeng Peng[a], Wang Xianchun[b], and Zeng Xiongzhi[b]

[a]Laboratory of Biological Engineering, College of Pharmacy, Hunan University of Chinese Medicine, Changsha, Hunan 410208, P. R. China; [b]Key Laboratory of Protein Chemistry and Developmental Biology of Ministry of Education, College of Life Sciences, Hunan Normal University, Changsha, Hunan 410081, P. R. China

ABSTRACT

JZTX-V is a toxin isolated from the venom of the Chinese spider *Chilobrachys jingzhao*. Previous studies had shown that JZTX-V could inhibit the transient outward potassium current of Kv4.2 and Kv4.3 expressed in *Xenopus* oocytes but had no effects on Kv1.2–1.4. However, the underlying action mechanism of JZTX-V on Kv4.3 remains unclear. In our study, JZTX-V could inhibit not only transient outward potassium currents evoked in small-sized DRG neurons but also Kv4.3-encoded currents expressed in HEK293T cells in the concentration and voltage dependence. The half maximal inhibitory concentration of JZTX-V on Kv4.3 was 9.6 ± 1.2 nM. In addition, the time course for JZTX-V inhibition and release of inhibition after washout were 15.8 ± 1.54 s and 58.8 ± 4.35 s. Electrophysiological assays indicated that 25 nM JZTX-V could shift significantly the voltage dependence of steady-state activation and steady-state inactivation to depolarization. Meanwhile, 25 nM JZTX-V decreased markedly the time constant of activation and inactivation but had no effect on the time constant of recovery from inactivation. To study the molecular determinants of Kv4.3, we performed alanine scanning on a conserved motif of Kv4.3 and assayed the affinity between mutants and JZTX-V. The results not only showed that I273, L275, V283, and F287 were molecular determinants in the conserved motif of Kv4.3 for interacting with JZTX-V but also speculated the underlying action mechanism that the hydrophobic interaction and steric effects played key roles in the binding of JZTX-V with Kv4.3. In summary, our studies have laid a scientific theoretical foundation for further research on the interaction mechanism between JZTX-V and Kv4.3.

ARTICLE HISTORY
Received 20 October 2021
Revised 1 March 2022
Accepted 1 March 2022

KEYWORDS
JZTX-V; kv4.3; mutants; molecular determinants; electrophysiological assays

Introduction

Potassium ion (K^+) channels are important to many biological processes and functions, for instance, action potential, neurotransmitters release, nerve conduction, blood pressure regulation, and so on [1,2]. Among the studied ion channels, K^+ channels are one of the most abundant ion channels. According to the spatial structure and physiological function of K^+ channels, they are mainly divided into five subfamilies, including the potassium channel with the pore-forming domain only (KcsA), voltage-gated, inwardly rectifying, tandem pore domain, and ligand-gated ones [3]. Voltage-gated potassium (Kv) channels are a kind of widely studied ion channels, which are composed of four α subunits and four β subunits. Each α subunit contains voltage-sensing domain and pore domain, in which transmembrane segments (S1-S4) and linkers between them constitute voltage-sensing domain, while the pore domain includes S5, S6, P-loop ion selectivity filters and linkers [4]. Of the voltage-sensing domains, only S4 contains positively charged arginine or lysine residues. Therefore, when the membrane potential depolarizes, the positively charged S4 moves through the gating canal and mediates the actual opening of the channels [4,5]. According to the properties of Kv channels, they are divided into 12 subtypes, of which the Kv4 subtype is encoded by the KCND gene family [6]. Kv4.1, Kv4.2, and Kv4.3 belong to Kv4 subtype, which are highly conserved in the transmembrane region while different at the amino terminal and carboxyl terminal [7]. Kv4.3 widely distributes in central neurons, peripheral neurons, and myocardial cells. It can be activated by the low voltage to produce the current, which is referred to as fast transient outward potassium current ($I_{A,fast}$ or $I_{A,f}$) due to

CONTACT Wang Xianchun wangxc@hunnu.edu.cn; Zeng Xiongzhi zengxz@hunnu.edu.cn Key Laboratory of Protein Chemistry and Developmental Biology of Ministry of Education, College of Life Sciences, Hunan Normal University, Changsha, Hunan 410081, P. R. China

characteristics of fast activation and fast time-dependently inactivation [7]. According to related studies, the current produced by Kv4.3 is the main component of myocardial potassium current (I_{to}) and small-sized dorsal root ganglion (DRG) neurons A-type potassium current (I_A) [8–10], of which abnormal performance will mainly lead to neurological and cardiovascular diseases [11]. Therefore, the research and development on related target drugs of Kv4, including Kv4.1–3, have positive significance for the treatment of various ion channelopathies caused by them.

Spiders are ancient creatures on the earth. In the long process of evolution, they have gradually acquired venom as a powerful weapon in order to catch prey and guard against natural enemies. Spider venom produced by its poisonous glands is a cocktail-like solution, mainly including low molecular weight organic matter (<1 kDa), small molecular disulfide-rich polypeptide (generally containing 3–6 pairs of disulfide bonds, with a molecular weight of about 1–10 kDa), nucleotides (such as ATP, ADP, and AMP), various free amino acids, and proteins (including various enzymes, with a molecular weight of about 10–120 kDa) [12]. Because it is complex and rich in various substances, spider venom has become a treasure trove for exploring bioactive substances, such as pharmacological research tools, drug lead molecules, biological pesticides, and so on [13,14]. A variety of spider venoms have been explored by various experimental techniques, and a large number of proteins or peptide toxins with biological activity have been isolated from the venom, including the toxins that act on Kv channels and regulate their gating properties. Spider toxins can be divided into two categories according to the different regions they act on in Kv channels. The one is pore-blocking toxins, which bind to the outer vestibule of Kv channels and inhibit the ion flow, such as Agitoxin2 and charybdotoxin [15,16]. The other one is gating-modifier toxins that interact with the voltage-sensing domain and modify voltage-dependent gating, including HaTx2, SgTx1, PaTx1, HpTx2, HmTx2, and so on [17]. JZTX-V is a spider toxin isolated from the venom of the Chinese rare spider *Chilobrachys jingzhao* [18]. It consists of 29 amino acid residues with a relative molecular weight of 3605.73 Da. The mature peptide of JZTX-V contains three pairs of disulfide bonds to form the inhibitor cystine knot (ICK) motif, of which sequence has different degrees of similarity with the gating-modifier toxins of Kv channels, especially highest similarity with PaTx1 to 83% (Figure 1). Previous studies had shown that JZTX-V could inhibit the transient outward potassium current of Kv4.2 and Kv4.3 expressed in *Xenopus* oocytes but had no effects on Kv1.2–1.4 [18–20]. In addition, of the two toxins with high similarity with JZTX-V, PaTx1 inhibits Kv4.2 and Kv4.3 currents, while HpTX2 plays effects by regulating a conserved motif of Kv4.3, consisting of transmembrane segment S3b and S3-S4 loop [21,22]. As a result, it may be reasonable to speculate that JZTX-V acts as a gating modifier by interacting with the conserved motif of Kv4.3.

To date, the mechanism of interaction between JZTX-V and Kv4.3 has not been deeply studied. In this study, we have characterized the mechanism of JZTX-V binding to the Kv4.3 expressed in HEK293T, and performed alanine scanning on the S3b-S4 voltage-sensing domain of Kv4.3 to study the interaction between JZTX-V and mutants. Our results will collectively support the

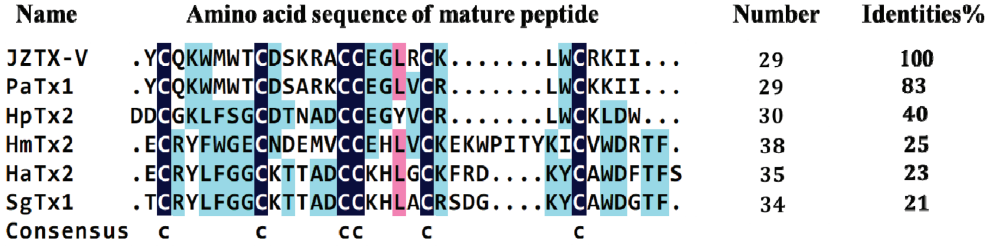

Figure 1. Alignment of JZTX-V with five gating-modifier toxins of Kv channels. Strictly conserved cysteines are indicated by deep blue and other less conserved amino acids are marked using different colors. PaTx1(UniProtKB ID = P61230), HpTx2(UniProtKB ID = P58426), HmTx2(UniProtKB ID = P60993), HaTx2(UniProtKB ID = P56853) and SgTx1(UniProtKB ID = P56855) were from *Phrixotrichus auratus, Heteropoda venatoria, Heteroscodra maculate, Grammostola spatulate* and *Scodra griseipes*, respectively.

utility of JZTX-V as a potential novel tool for studying Kv4, including Kv4.1–3, and ion channelopathies caused by them.

Materials and methods

Chemical synthesis of JZTX-V

The solid-phase synthesis of JZTX-V was carried out by referring to the methods of Zeng et al. [23], of which steps are briefly described as follows. First, according to the primary sequence of JZTX-V, the Fmoc-protected amino acids were used to synthesize the liner JZTX-V on the PS3™ automated peptide synthesizer (Protein Technologies, USA). Second, the synthetic linear peptide was oxidatively refolded. Finally, the end product was purified by HPLC (Waters, USA) to 99% purity.

Site-directed mutagenesis of wild-type Kv4.3

Professor David Mckinnon of New York State University of the USA kindly provided rat wild-type Kv4.3 (NCBI accession number Q62897.2) that subcloned into pcDNA3.1 vector. The alanine scanning on the S3b-S4 voltage sensing domain of Kv4.3 was constructed by GeneTailor™ Site-Directed Mutagenesis System: For standard and high-throughput in vitro site-directed mutagenesis (Invitrogen, USA) and confirmed by sequencing (Beijing Genomics Institute, China).

Isolation, culture, and transient transfection of cells

DRG neurons were acutely dissociated from Sprague–Dawley (SD) rats as previously described [24]. DRG neurons with diameters of less than 10 mm were selected to study K^+ channels, since small-sized DRG neurons tend to express Kv4.3 [8]. SD rats (Hunan SJA Laboratory Animal Co., Ltd., China) were used according to the guidelines of the National Institutes of Health for Care and Use of Laboratory Animals. The experiments were approved by the Animal Care and Use Committee of Hunan Normal University.

The human embryonic kidney 293 T cell line (HEK293T) was obtained from Shanghai Institute of Cell Biology (Chinese Academy of Sciences, China) and maintained in DMEM (Invitrogen, USA) supplemented with 10% heat-inactivated fetal calf serum (Gibco™, USA), penicillin (100 U/ml, Sangon biotech, China), and streptomycin (100 μg/ml, Sangon biotech, China). Wild-type Kv4.3 or all of the mutants were transiently co-transfected into HEK293T cells, with eGFP using the Lipfectamine™2000 Reagent (Invitrogen, USA). The cells that had green fluorescence were selected to electrophysiological assays.

Electrophysiological assays

Voltage-clamp recording was performed with whole-cell patch clamp techniques using an EPC-9 patch clamp amplifier (HEKA Electronics, Germany), and all measurements were carried out at room temperature (25°C). The resistance of microelectrodes filled with internal solution was 2–3 MΩ. Series resistance compensation was set at 80%. The isolated DRG neurons were plated on 35 mm Petri dishes (Sigma, USA) and incubated in CO_2 incubator for 3 h before the patch clamp experiments. The transfected HEK293T cells were transferred into 35 mm Petri dishes 1 day before electrophysiological assays. The external solution and internal solution for DRG and HEK293T were used as follows.

For DRG, the internal solution contained (in mM): 120 KF, 20 N-methyl-D-glucamine, 10 HEPES, 11 EGTA, 2 Mg-ATP, 0.5 GTP-2Li (pH = 7.2, Sangon biotech, China). The external solution contained (in mM): 130 Choline chloride, 5 KOH, 10 HEPES, 12 Glucose, 2 $MgCl_2$, 2 $CaCl_2$ (pH = 7.2, Sangon Biotech, China).

For HEK293T, micropipettes were filled with an internal solution containing KF 140 mM, ATP-2Na 5 mM, EGTA 1 mM, HEPEs 10 mM (pH = 7.4, Sangon biotech, China). The external solution contained NaCl 137 mM, KCl 5.9 mM, $CaCl_2$ 2.2 mM, $MgCl_2$ 1.2 mM, glucose 14 mM, HEPEs 10 mM (pH = 7.4, Sangon biotech, China).

In the study, the stock solution concentration of JZTX-V was 1 mM and could be diluted to the needed concentration with the external solution. 4-Aminopyridine (4-AP, Sangon biotech, China) was prepared at a concentration of 10 mM with the external solution.

Data analysis and three-dimensional structure construction

The data analysis was performed using Pulsefit (HEKA Electronics) and Origin 7.5. All data are presented as means ± SD, and n is the number of independent experimental cells. Significant difference was compared by Student's t-test. The 3D structure information of the toxin peptides was obtained from the PDB database, and their 3D structures were constructed using VMD software (version 1.9.2).

Results

Inhibition effects of JZTX-V on K^+ currents in rat small-sized DRG

The small-sized DRG neurons were selected to evoke K^+ currents, which were recorded in response to +30 mV depolarization, preceded by prepulses of −80 mV. 10 mM 4-AP and 1 μM JZTX-V were applied to the evoked K^+ currents, respectively. The results showed that both 4-AP and JZTX-V could inhibit K^+ currents (Figure 2(a,b)), in which the inhibition rate of 4-AP was 70 ± 3%, while that of JZTX-V was 45 ± 5%. According to these results, we point out that JZTX-V can inhibit I_A mainly encoded by Kv4.3 in small-sized DRG neurons.

Inhibition effects and characteristics of JZTX-V on wild-type Kv4.3 expressed in HEK293T cells

Under the −80 mV holding voltage and +10 mV stimulation voltage, HEK293T cells containing wild-type Kv4.3 plasmids were detected by a patch clamp. The results showed that transient outward potassium current could be recorded (Figure 3(a)), indicating that wild-type Kv4.3 was successfully expressed in the HEK293T cell membrane. Then, in order to study the biological effect of JZTX-V on Kv4.3, HEK293T cells were treated with different concentrations of JZTX-V under the same patch clamp conditions. The results showed that with the increase of JZTX-V concentration, Kv4.3 currents gradually decreased (Figure 3(a)). It could be concluded that the inhibition effect of JZTX-V on wild-type Kv4.3 currents was concentration-dependent, and its half maximal inhibitory concentration (IC_{50}) was 9.6 ± 1.2 nM (Figure 3(b)).

As shown in Figure 3(c), 100 nM JZTX-V had different inhibition percentages at +10 mV and +50 mV (94% at +10 mV and 57% at +50 mV). The inhibition percentage of JZTX-V was smaller and smaller with the increase of test potential from −30 mV to +60 mV (Figure 3(d)), suggesting that the inhibition of wild-type Kv4.3 current by JZTX-V was voltage-dependent. We measured the time course for JZTX-V inhibition of Kv4.3 current (τ_{on}) and the time course for release of inhibition after washout of the toxin (τ_{off}). Figure 3(e) shows the time course of inhibition during application of 100 nM JZTX-V and after washout. The on and off rates were 15.8 ± 1.54 s and 58.8 ± 4.35 s by fitting with exponential functions, respectively.

Effects on activation, inactivation, and recovery kinetics of wild-type Kv4.3 by JZTX-V

HEK293T cells were held at −80 mV, and then a series of continuous pulses ranging from −80 mV to +60 mV was given in +10 mV

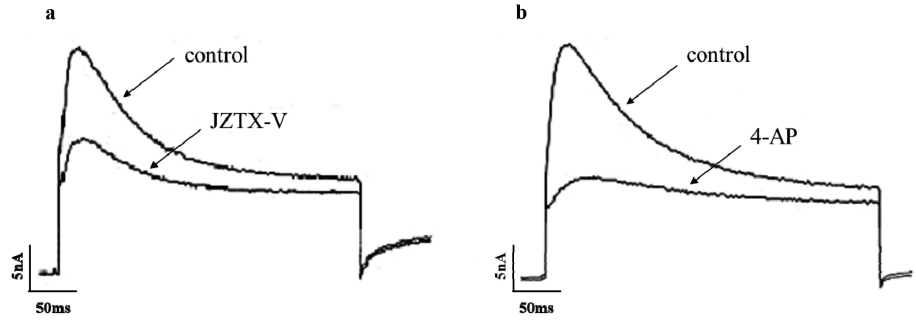

Figure 2. The effects of JZTX-V and 4-AP on the K^+ currents in rat small-sized DRG. (a) The inhibition effects of 1 μM JZTX-V. (b) The inhibition effects of 10 mM 4-AP.

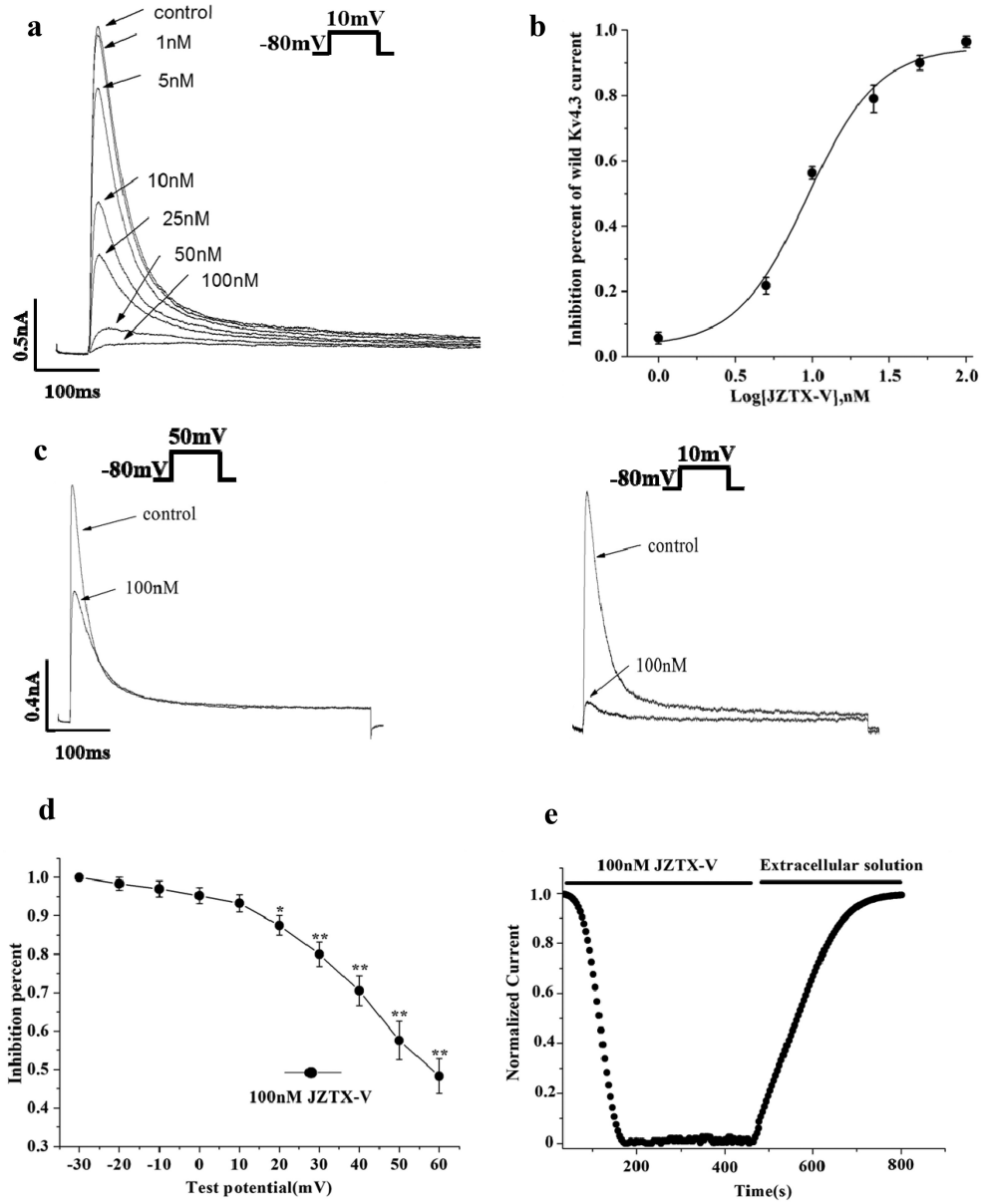

Figure 3. The characteristics of JZTX-V to wild-type Kv4.3 expressed in HEK293T cells. (a)The inhibition effect of JZTX-V on Kv4.3 current. With the increase of JZTX-V concentration, Kv4.3 current gradually decreased. (b) The dose–inhibition curve. It was fitted by the Hill logistic equation: Inhibition% = $(A_1\text{-}A_2)/ [1 +(x/x_0)^{p}] +A_2$, in which A_1, A_2, x, x_0 and p was the initial value of inhibition, final value of inhibition, JZTX-V concentration, IC_{50} and power, respectively. The IC_{50} is 9.6 ± 1.2 nM. (c) The effect of 100 nM JZTX-V on Kv4.3 current recorded at +10 nM and +50 nM, respectively. The inhibition percentage of 100 nM JZTX-V on wild-type Kv4.3 current at +10 mV (94%) is higher than at +50 mV (57%). (d) The Voltage–inhibition curve. At each potential, the peak amplitude of current in the presence of JZTX-V was normalized to that in the absence of JZTX-V. The inhibition of Kv4.3 current by JZTX-V was voltage dependent (*P < 0.05 or ** P < 0.01 Vs −30 mV). (e) Time course of inhibition of Kv4.3 with 100 nM JZTX-V and recovery from inhibition. The two bars indicate the duration of 100 nM JZTX-V application and washout, respectively. The pulse protocol started from a holding potential of −80 mV followed by a pulse to 10 mV for 150 ms with a 1 s interpulse interval. The data represent the normalized reciprocal current amplitude measured from the maximum of the pulse. The on and off rates were fit with the functions f_{on} (t) = C× exp(-t/τ_{on}) and f_{off} (t) = C×[(1-exp(-t/τ_{off})]^4, respectively. All data were presented as means ±SD, and came from 4 ~ 6 independent cell experiments.

increments, which resulted in currents as shown in Figure 4(a). The current peak amplitude under each depolarizing pulse was normalized by the maximal current generated in the absence of JZTX-V and at +60 mV pulse. After normalization, each dot was plotted against the corresponding depolarizing pulse, and then fitted to form steady-state activation curves (Figure 4(b)). As

shown in Figure 4(b), 25 nM JZTX-V shift significantly the half-maximal active potential ($V_{0.5}$ act.) to depolarization, of which detailed change data are shown in Table 1.

The double-pulse protocol was employed to further study the effects of JZTX-V on the steady-state inactivation curves of wild-type Kv4.3. HEK293T cells were held by a series of

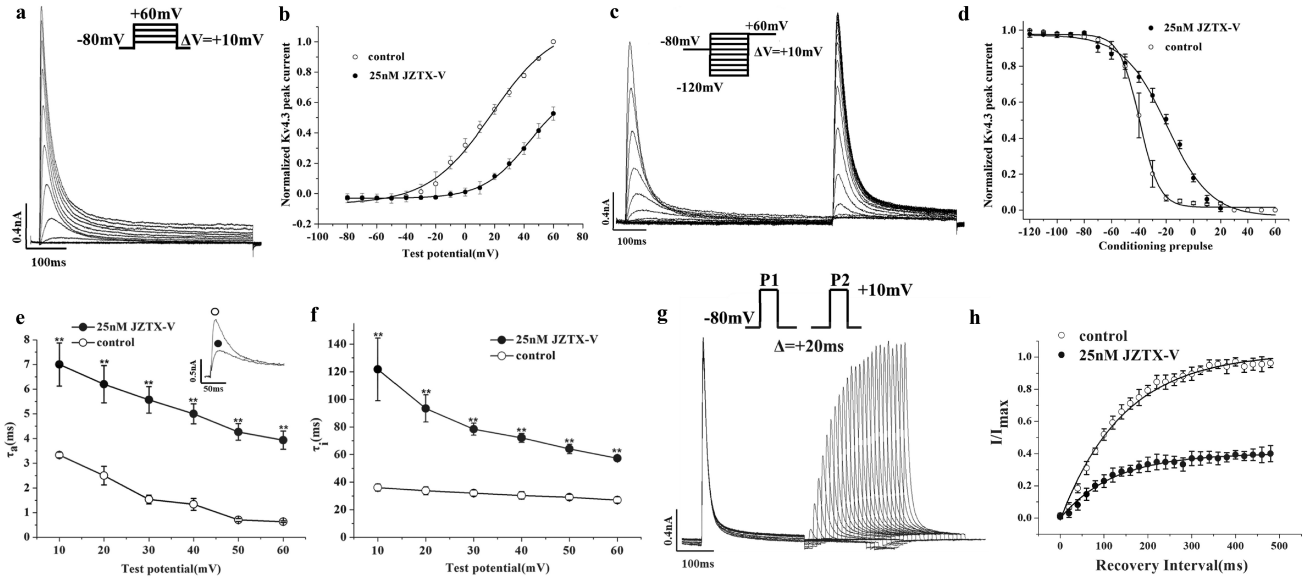

Figure 4. The effects of JZTX-V on activation, inactivation and recovery kinetics of wild-type Kv4.3 current. (a)Current diagram of steady-state activation. In the absence of JZTX-V, K^+ current was elicited by depolarization ranging from −80 mV to +60 mV in +10 mV increments. (b)Steady-state activation curves. It was fitted by the equation: $I/I_{max} = 1/ [1+ \exp (V_{0.5}\text{-}V)/k]$, in which $V_{0.5}$ was half-maximal active potential, k was the slope factor and I_{max} was the maximal current generated in the absence of JZTX-V and at +60 mV pulse. (c)Current graph of steady-state inactivation. In the absence of JZTX-V, double-currents were evoked by double-pulses including conditioning prepulse ranging from −120 mV to +60 mV and depolarizing pulse at +60 mV. (d) Steady-state inactivation curves. It was fitted by the equation: $I/I_{max} = 1/ [1+ \exp -(V_{0.5}\text{-}V)/k]$, in which $V_{0.5}$ is half-maximal inactive potential, k is the slope factor and I_{max} is the maximal current evoked by P2. (e) τ_a in absence and presence of JZTX-V at different potential ranging from +10 mV to +60 mV. The rising phase of the wild-type Kv4.3 current was fitted by the equation: $I(t) = I_0 + A_1[1\text{-}\exp(-t/\tau_a)]$, in which τ_a was the activation time constant (*P < 0.05 or ** P < 0.01 Vs absence of JZTX-V at each potential). The inset shows the effect of JZTX-V at +20 mV. (f) τ_i in absence and presence of JZTX-V at different potential ranging from +10 mV to +60 mV. The decay phase of the wild-type Kv4.3 current was fitted by the equation: $I(t) = I_0 + A_1\exp [-(t\text{-}t_0)/\tau_i]$, in which τ_i was the inactivation time constant (*P < 0.05 or ** P < 0.01 Vs absence of JZTX-V at each potential). (g) Current traces of Kv4.3 recovery from inactivation recorded by the single cell. The HEK293T cell was depolarized by double-pulse (P1 to +10 mV, with holding potential = −80 mV, followed by P2 to +10 mV), while interpulse interval between them was allowed to vary from 0 to 500 ms in 20 ms increments. (h) τ_r in absence and presence of JZTX-V at different recovery intervals. Peak currents elicited by test pulse(P2) were plotted as a function of time and data points were fitted by equation: $I(t) = I_0 + A_1[1\text{-}\exp(-t/\tau_r)]$, in which τ_r was the recovery time constant. All data(b, d~f, and h) were presented as means ±SD, and came from 6 independent cell experiments.

Table 1. Effects of JZTX-V on kinetic parameters of Kv4.3 channels.

Parameters	Control (test pulse in mV)	25 nM JZTX-V	P
$V_{0.5}$ act. in mV ± SD n = 6	18.3 ± 1.5	42.3 ± 0.9**	0.0003
$V_{0.5}$ inact. in mV ± SD n = 6	−40 ± 3.2	−22 ± 2**	0.003
τ_a in ms ± SD n = 6	1.4 ± 0.2(40 mV)	5 ± 0.4**	0.002
τ_i in ms ± SD n = 6	30.3 ± 2.7(40 mV)	72 ± 3.2**	0.001
τ_r in ms ± SD n = 6	141 ± 18	116 ± 16	0.34
**P < 0.01 Vs control			

All data are presented as means ± SD, and *n* was the number of independent experiments. $V_{0.5}$ act. was half-maximal active potential. $V_{0.5}$ inact was half-maximal inactive potential. τ_a was the activation time constant. τ_i was the inactivation time constant. τ_r was the recovery time constant.

conditioning prepulses ranging from −120 mV to +60 mV in 10 mV increments (P1) and then tested at +60 mV (P2)(Figure 4(c)). The current peak amplitude under each P2 was normalized by the maximal current at P2. After normalization, each dot was plotted against the corresponding P1, and then fitted to form steady-state inactivation curves (Figure 4(d)). As illustrated in Figure 4(d), 25 nM JZTX-V shift significantly the half-maximal inactive potential ($V_{0.5}$ inact.) to depolarization, of which detailed change data are shown in Table 1.

According to the current data obtained from the steady-state activation mode, the rising phase and decay phase of the wild-type Kv4.3 current were fitted by the corresponding single exponential equation to calculate the activation time constant (τ_a) and inactivation time constant (τ_i). As shown in Figure 4(e,f) and Table 1, 25 nM JZTX-V can significantly delay the τ_a and τ_i of the wild-type Kv4.3 current under various voltage stimuli.

A double-pulse protocol, that conditioning pulse (P1) and test pulse (P2) were set at +10 mV while the interpulse interval between them was changed in 10 ms increments, was applied to the HEK293T cells expressing wild-type Kv4.3 (Figure 4(g)). The current peak amplitude under P2 was normalized by the maximal current generated in the absence of JZTX-V and at P1. After normalization, each dot was plotted against the corresponding recovery interval, and then fitted to form inactivation recovery curves. As illustrated in Figure 4(h), at least 500 ms were required for wild-type Kv4.3 to recover from inactivation. Compared with control, recovery time constant (τ_r) of wild-type Kv4.3 channels was not significantly modified by 25 nM JZTX-V (Table 1).

Molecular determinants of Kv4.3 for interacting with JZTX-V

To study the molecular determinants of Kv4.3 for interacting with JZTX-V, the alanine scanning was performed on the conserved motif of Kv4.3 consisting of transmembrane segment S3b and S3-S4 loop (Figure 5(a)). And then, the concentration–effect relationship between JZTX-V and mutants was assayed. As illustrated in Figure 5(b-d), alanine scanning on the conserved motif of Kv4.3 nearly had no effects on the concentration–effect relationship between JZTX-V and Kv4.3, except for I273A, L275A, V283A, and F287A, of which V283A and F287A significantly decreased affinity for JZTX-V, while I273A and L275A significantly increased affinity for JZTX-V. The results indicated that these residues on K_V4.3 are involved in the binding of JZTX-V.

Discussion

Animal toxins are good tools to study ion channels, and many toxins have been applied to research the regulation mechanism of ion channels. As a spider-venom toxin, JZTX-V has some specificity on Kv channels. According to the existing experimental results, the molecule only had inhibitory effects on Kv4.2 and Kv4.3 expressed in *Xenopus* oocytes, but no effects on other Kv channels, such as Kv1.2–1.4 [18–20]. To further determine whether JZTX-V acted on the Kv4.3-encoded currents in native cells, we chose small-sized DRG neurons and 4-AP as the research object and research tool to explore this problem, respectively. According to the report by Matsuyoshi [8], I_A in small-sized DRG neurons is mainly encoded by Kv4.3. When small-sized DRG neurons were depolarized with +30 mV under the condition of −80 mV holding potential, a composite current consisting of $I_{A,f}$ and delayed rectified potassium current (I_K) could be evoked, in which $I_{A,f}$ was specifically inhibited by 4-AP, while I_K was not sensitive to 4-AP [25]. On this basis, we detected the effect of JZTX-V on K^+ current in small-diameter DRG neurons using the whole-cell patch-clamp detection. As shown in Figure 2, JZTX-V inhibited $I_{A,f}$ as well as 4-AP, which proved that JZTX-V could inhibit the Kv4.3-encoded currents in native cells. In this study, the effects of JZTX-V on the wild-type Kv4.3 current expressed in HEK293T cells were studied. The results showed that the IC_{50} (9.6 ± 1.2 nM) of Kv4.3 inhibited by JZTX-V was smaller than the IC_{50} (13 ± 1.7 nM) of Kv4.2 [19]. Moreover, under the same detection conditions, it was also lower than other animal toxins that inhibited Kv4.3, such as Ctri9577 (IC_{50} = 1.34 ± 0.03 μM) [26]. In addition, the inhibitory effect of JZTX-V on Kv4.3 was voltage-dependent,

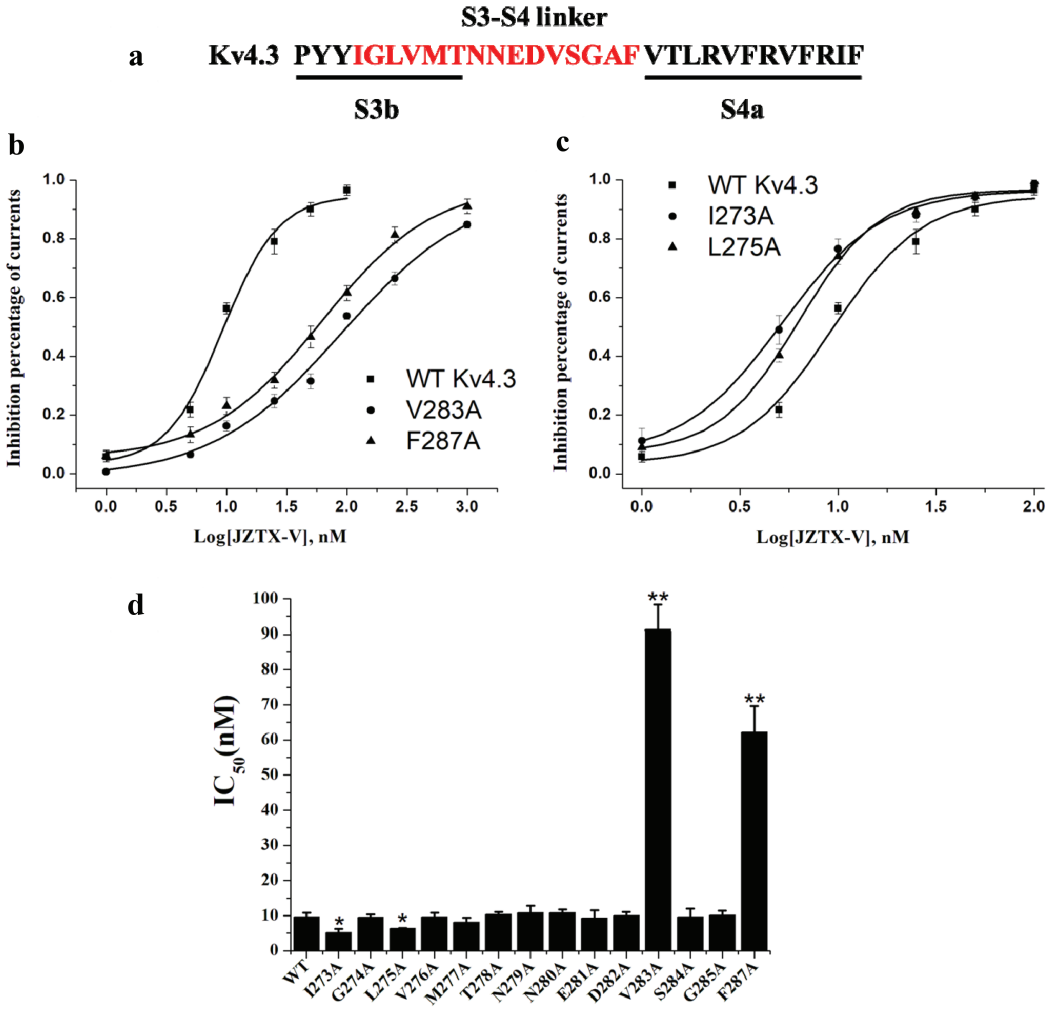

Figure 5. Inhibitory Effect of JZTX-V on Alanine mutants of S3b-S4 region in Kv4.3 voltage-sensing domain. (a) Alanine scanning on voltage-sensing domains of Kv4.3. Amino acid residues marked in red were replaced by alanine. (b) The dose–inhibition curves of V283A and F287A. Mutation of V283A and F287A reduced sensitivity to the JZTX-V by ~10-and~ 6-fold with IC_{50} of 91.3 ± 7.0 and 62.2 ± 7.4 nM, respectively. (c) The dose–inhibition curves of I273A and L275A. The IC_{50} of I273A and L275A were 5.1 ± 1.1 nM and 6.3 ± 0.2 nM, respectively. (d) Histogram of IC_{50} value for each mutant. The affinity of mutants, V282A and F286A, to JZTX-V decreased significantly, while the affinity of I273A and L275A to JZTX-V increased significantly (*P < 0.05 or ** P < 0.01 Vs wild-type Kv4.3). All data were presented as means ±SD, and came from 4 ~ 6 independent cell experiments.

which also existed in other studies of spider toxins, for instance the interactions between HaTx1 and Kv2.1, PaTx1 and Kv4.3, HpTx2 and Kv4.2, respectively [21,27,28]. The auxiliary subunit (KChIP2b) is often co-expressed with the native Kv4.3 channel, which affects the gating behavior of toxins. For instance, DeSimone et al. evaluated the affinity of HpTx2 for Kv4.3 co-expressed with KChIP2b to better understand Kv4.3-based transient outward currents in natural tissues. The results showed that KChIP2b increased affinity between the toxin and channel by stabilizing the closed state of Kv4.3 [22]. JZTX-V and HpTx2 have many similarities in structure and function. For instance, JZTX-V is similar to HpTx2 in the amino acid sequence (Figure 1). In addition, the two toxins act with Kv4.3 in a voltage-dependent manner and recovery from inhibition by elution. Accordingly, we speculate that the effects of JZTX-V on Kv4.3 are the same as HpTx2 to be influenced by KChIP2b.

Through sequence alignment, it was found that JZTX-V had high sequence similarity with some spider toxins previously reported, of which the highest similarity with PaTx1, a typical gating-modifier toxin for Kv channels. In this research, therefore, the

gating properties of JZTX-V on wild-type Kv4.3 were studied. The results indicated that JZTX-V could change the gating properties of wild-type Kv4.3 and made its semi-activation voltage and semi-deactivation voltage shift significantly toward depolarization. Besides, JZTX-V could significantly delay the activation and inactivation time constant of the transient outward potassium current of wild-type Kv4.3, but has no significant effect on the inactivation recovery time constant of the currents. The above results are similar to the gating properties of PaTx1, so it is reasonable to conclude that JZTX-V is also a gating-modifier toxin for Kv4.3.

The voltage sensor trapping mechanism may be a common mode of action for polypeptide gating-modifier toxins acting on all of Kv channels [29,30], of which theory can be summarized as follows: (1) The sensors in voltage-dependent K^+ channels are located at the membrane–protein interface [2,31,32]; (2) The molecular surfaces of gating-modifier toxins usually have a large hydrophobic patch surrounded with charged residues (Figure 6), of which is helpful for toxins to be located at the interface between polar head groups and the hydrophobic phase of the membrane. (3) Through the membrane partitioning mechanism, the toxins are distributed from the aqueous solution to the cell membrane for enrichment, and then diffused laterally until they found and directly bound to the sensor in voltage-dependent K^+ channels [33,34]. Further studies showed that some toxins trapped the voltage sensor of Kv channels by directly interacting with a conserved motif of Kv channels, consisting of transmembrane segment S3b and S3-S4 loop [17,35,36]. For example, the affinity of HpTx2 and Ctri9577 to Kv4.3 was influenced by the transmembrane segment S3b, and VSTx1 could influence its binding to KvAP through the S3-S4 loop [22,26,30]. According to the aforementioned reports, our study used site-directed mutation technology to carry out alanine scanning on the transmembrane segment S3b and the S3-S4 loop of Kv4.3, and determined the IC_{50} of JZTX-V on Kv4.3 mutants to deduce the molecular determinants of the interaction between them. As shown in results, the mutation of four amino acid residues (I273, L275, V283,

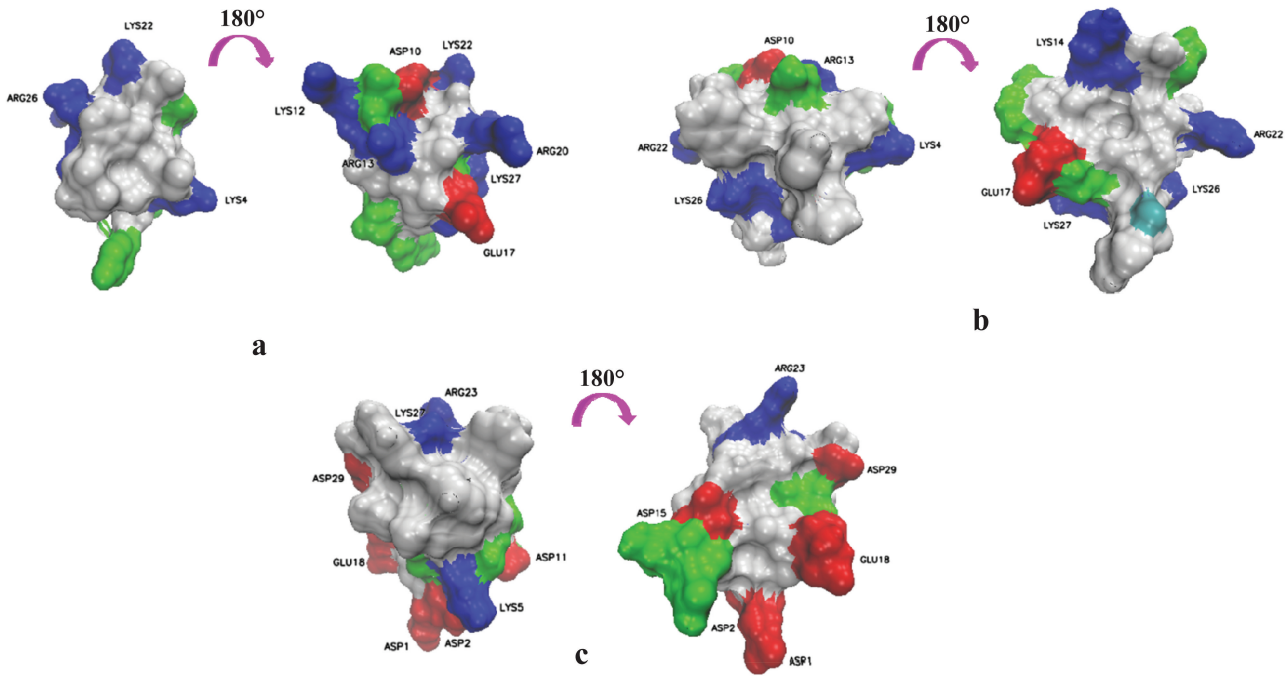

Figure 6. Three-dimensional structure of JZTX-V, PaTx1 (1V7F) and HpTx2(1EMX). (a), (b) and (c) are JZTX-V (PDB code 6CHC), PaTx1 (PDB code 1V7F) and HpTx2(PDB code 1EMX), respectively. In (a), (b) and (c), the left is the side containing the hydrophobic patch, and the right is the 180° rotation side containing the charged residues and surrounding the hydropathic patch. Residues are colored according to their properties. Blue, basic (Arg, Lys, His); Red, acidic (Glu, Asp); Green, Polarity uncharged (Ser, Thr, Tyr, Gln, Asn, Cys and Gly); White, hydrophobic (Ala, Ile, Leu, Met, Phe, Pro, Trp and Val).

and F287), respectively, into alanine could significantly affect the affinity of JZTX-V to Kv4.3, of which I273 and L275 increased affinity, while V283 and F287 decreased it. The above experimental results, on the one hand, further verified that the conserved motif of Kv4.3 was a key region for toxins to interact with Kv4.3 and regulate its gating properties. On the other hand, it could also explain some mechanisms of affinity between JZTX-V and K4.3. Zeng et al. modeled the spatial structure of JZTX-V according to the three-dimensional structure of PaTx1 [18]. From the constructed structure, it could be found that JZTX-V had a large hydrophobic patch consisting of three aromatic residues and two aliphatic residues (Figure 6). The hydrophobic patch might interact with the hydrophobic residues (V283, and F287) found in the conserved motif of Kv4.3 to achieve mutual binding between toxins and channels. However, if the hydrophobic residues were mutated into neutral alanine, the hydrophobic interaction would be weakened, which affected the mutual binding between toxins and channels. Meanwhile, decreasing the side chain volume/size at positions 273 and 275 (A instead of I and L) may produce beneficial steric effects for toxin binding. In addition, although other toxins could also interact with the conserved motif of Kv4.3, the molecular determinants were not identical. For example, the molecular determinants targeted by HpTx2 in the conserved motif were L275, V276, and N280 [22], while Ctr9577 was L275, V276, N280, and V288 [26]. Therefore, it could be seen that in regulating the gating properties of Kv4.3, JZTX-V not only has the conservation of action region but also has the uniqueness of molecular determinants. It is worth noting that the effects of alanine mutation on the kinetics of the channels, the kinetics of toxin–channel interaction and allosteric effects on channel gating are not studied in this work. Accordingly, we will further explore these issues to deepen our understanding of the interaction mechanism between JZTX-V and Kv4.3 in our future work.

Conclusion

In conclusion, JZTX-V is a kind of gating-modifier toxin for Kv channels with good specificity, which may realize gated regulation through hydrophobic interaction and steric effects with the conserved motif of Kv4.3. Accordingly, JZTX-V is expected to be developed as a novel tool for studying the normal physiological functions of Kv4, including Kv4.1–3, and the ion channelopathies caused by their abnormal conditions.

Acknowledgments

We thank professor David Mckinnon for providing rat wild-type Kv4.3 gene that subcloned into pcDNA3.1 vector.

Disclosure statement

No potential conflict of interest was reported by the author(s).

Funding

This work was supported by the National Natural Science Foundation of China (82104324, 31271135, 31070700), Scientific Research Project of Hunan Provincial Department of Education (19C1407), Scientific Research Foundation of Hunan University of Traditional Chinese Medicine (2020XJJJ030), The key discipline of biological engineering of Hunan University of Chinses medicine ([2018] No.3), and Scientific Research Foundation of Hunan Key Laboratory of Chinese Materia Medica Powder and Innovative Drugs Established by Provincial and Ministry ([2020] No.1).

Data availability

The data used to support the findings of this study are available from the corresponding author upon request.

Author Contributions

Dehong Xu and Xiongzhi Zeng designed the research. Dehong Xu, Wenmei Wu, Siqin Hong, Peng Zeng performed the experiments and analyzed the data. Dehong Xu wrote the manuscript. Xiongzhi Zeng and Xianchun Wang supervised this work and revised the manuscript.

References

[1] Armstrong CM, Hollingworth S. Na+ and K+ channels: history and structure. Biophys J. 2021;120 (5):756–763.

[2] González C, Baez-Nieto D, Valencia I, et al. K (+) channels: function-structural overview. Compr Physiol. 2012;2:2087–2149.

[3] Kuang Q, Purhonen P, Hebert H. Structure of potassium channels. Cell Mol Life Sci. 2015;72 (19):3677–3693.

[4] Abbott GW. KCNQs: ligand- and Voltage-Gated Potassium Channels. Front Physiol. 2020;11:583–599.

[5] Kim DM, Nimigean CM. Voltage-Gated Potassium Channels: a Structural Examination of Selectivity and Gating. Cold Spring Harb Perspect Biol. 2016;8(5): a029231.

[6] Gutman GA, Chandy KG, Grissmer S, et al. International Union of Pharmacology. LIII. Nomenclature and molecular relationships of voltage-gated potassium channels. Pharmacol Rev. 2005;57(4):473–508.

[7] Birnbaum SG, Varga AW, Yuan LL, et al. Structure and function of Kv4-family transient potassium channels. Physiol Rev. 2004;84(3):803–833.

[8] Matsuyoshi H, Takimoto K, Yunoki T, et al. Distinct cellular distributions of Kv4 pore-forming and auxiliary subunits in rat dorsal root ganglion neurons. Life Sci. 2012;91(7–8):258–563.

[9] Huo R, Sheng Y, Guo WT, et al. The potential role of Kv4.3 K + channel in heart hypertrophy. Channels (Austin). 2014;8(3):203–209.

[10] Nerbonne JM. Molecular basis of functional voltage-gated K + channel diversity in the mammalian myocardium. J Physiol. 2000;525(2):285–298.

[11] Pollini L, Galosi S, Tolve M, et al. KCND3-Related Neurological Disorders: from Old to Emerging Clinical Phenotypes. Int J Mol Sci. 2020;21 (16):5802–5817.

[12] Langenegger N, Nentwig W, Kuhn-Nentwig L. Spider Venom: components, Modes of Action, and Novel Strategies in Transcriptomic and Proteomic Analyses. Toxins (Basel). 2019;11(10):611–655.

[13] Saez NJ, Herzig V. Versatile spider venom peptides and their medical and agricultural applications. Toxicon. 2019;158:109–126.

[14] Akef HM. Anticancer, antimicrobial, and analgesic activities of spider venoms. Toxicol Res (Camb). 2018;7(3):381–395.

[15] Ranganathan R, Lewis JH, MacKinnon R. Spatial localization of the K+ channel selectivity filter by mutant cycle-based structure analysis. Neuron. 1996;16 (1):131–139.

[16] Miller C. The charybdotoxin family of K+ channel-blocking peptides. Neuron. 1995;15(1):5–10.

[17] Swartz KJ. Tarantula toxins interacting with voltage sensors in potassium channels. Toxicon. 2007;49 (2):213–230.

[18] Zeng X, Deng M, Lin Y, et al. Isolation and characterization of Jingzhaotoxin-V, a novel neurotoxin from the venom of the spider *Chilobrachys jingzhao*. Toxicon. 2007;49(3):388–399.

[19] Zhang Y, Luo J, He J, et al. JZTX-V Targets the Voltage Sensor in Kv4.2 to Inhibit Ito Potassium Channels in Cardiomyocytes. Front Pharmacol. 2019;10: 357–367.

[20] Cai LJ, Xu DH, Luo J, et al. Inhibition of Jingzhaotoxin-V on Kv4.3 channel. Sheng Li Xue Bao. 2010;62(3):255–260.

[21] Diochot S, Drici MD, Moinier D, et al. Effects of phrixotoxins on the Kv4 family of potassium channels and implications for the role of I to 1 in cardiac electrogenesis. Br J Pharmacol. 1999;126(1):251–263.

[22] DeSimone CV, Lu Y, Bondarenko VE, et al. S3b Amino Acid Substitutions and Ancillary Subunits Alter the Affinity of Heteropoda venatoria Toxin 2 for Kv4.3. Mol Pharmacol. 2009;76(1):125–133.

[23] Zeng XZ, Deng MC, Sun ZH, et al. Synthesis, Refolding and Characterization of JZTX-Vand Its Effect on Potassium Channels. Chinese Journal of Biochemistry and Molecular Biology. 2008;24:463–468.

[24] Wang M, Diao J, Li J, et al. JZTX-IV, a unique acidic sodium channel toxin isolated from the spider *Chilobrachys jingzhao*. Toxicon. 2008;52(8):871–880.

[25] Rola R, Witkowski G, Szulczyk PJ. Voltage-dependent K^+ currents in rat cardiac dorsal root ganglion neurons. Neuroscience. 2003;119(1):181–191.

[26] Xie C, Li T, Xu L, et al. Kv1.3 potassium channel-blocking toxin Ctri9577, novel gating modifier of Kv4.3 potassium channel from the scorpion toxin family. Biochem Biophys Res Commun. 2014;444 (3):406–410.

[27] Swartz KJ, MacKinnon R. Hanatoxin modifies the gating of a voltage-dependent K+ channel through multiple binding sites. Neuron. 1997;18(4):665–673.

[28] Sanguinetti MC, Johnson JH, Hammerland LG, et al. Heteropodatoxins: peptides isolated from spider venom that block Kv4.2 potassium channels. Mol Pharmacol. 1997;51(3):491–498.

[29] Catterall WA, Cestèle S, Yarov-Yarovoy V, et al. Voltage-gated ion channels and gating modifier toxins. Toxicon. 2007;49(2):124–141.

[30] Lau CHY, King GF, Mobli M. Molecular basis of the interaction between gating modifier spider toxins and the voltage sensor of voltage-gated ion channels. Sci Rep. 2016;6(1):34333.

[31] Jiang Y, Ruta V, Chen J, et al. The principle of gating charge movement in a voltage-dependent K^+ channel. Nature. 2003;423(6935):42–48.

[32] Börjesson SI, Elinder F. Structure, function, and modification of the voltage sensor in voltage-gated ion channels. Cell Biochem Biophys. 2008;52(3):149–174.

[33] Wee CL, Gavaghan D, Sansom MS. Interactions between a voltage sensor and a toxin via multiscale simulations. Biophys J. 2010;98(8):1558–1565.

[34] Lee SY, MacKinnon R. A membrane-access mechanism of ion channel inhibition by voltage sensor toxins from spider venom. Nature. 2004;430 (6996):232–235.
[35] Shiau YS, Huang PT, Liou HH, et al. Structural basis of binding and inhibition of novel tarantula toxins in mammalian voltage-dependent potassium channels. Chem Res Toxicol. 2003;16(10):1217–1225.
[36] Li-SmerinY, SwartzKJ. Gating modifier toxins reveal a conserved structural motif in voltage-gated Ca 2+ and K + channels. Proc Natl Acad Sci USA. 1998;95 (15):8585–8589.